Received: September 6, 2022. Revised: November 23, 2022. 24

INASS

International Journal of
Intelligent Engineering & Systems

http://www.inass.org/

Hybrid Statistical and Texture Features with DenseNet 121 for Breast Cancer Classification

Gurusiddayya Hiremath[1]* Jose Alex Mathew[2] Naveen Kumar Boraiah[3]

[1]*Department of Electrical & Electronics Engineering,*
Sahyadri College of Engineering & Management, Mangalore, India
[2]*Department of Electrical & Electronics Engineering, Srinivasa Institute of Technology, Valachill, India*
[3]*Department of Information Science & Engineering,*
Sahyadri College of Engineering & Management, Mangalore, India
* Corresponding author's Email: Gurusiddayya.ec@sahyadri.edu.in

Abstract: Cancers are aggressive which is coupled with higher mortality rates and remain a major life-threatening factor in humans. Thus, early detection of cancer among patients is important as it showed a great survival chance. Therefore, early detection provides the patients with greater survival chances. The diagnosis performed for the mammography images are quite expensive and also radiations produced during the process were harmful to the patients. Thermography is a cost-effective and invasive method compared to mammography images and thus has reached its popularity. The present research is aimed to create the Machine Learning (ML) models using Convolutional Neural Networks (CNN) approaches which were created based on the machine learning models. The present research work utilized the DMR-IR dataset for the results evaluation and performance evaluation of the model which has been verified with datasets. The feature extraction process utilizes a machine learning algorithm to overcome the problems. The developed models were engaged in sophisticated ways to extract the features to improve the classification of the model. The Hybrid statistical and texture feature extraction technique extracts the features better in turn improved the model training. The results showed that the proposed hybrid feature extraction with the Dense Net 121 model obtained better accuracy of 98.97 %, the precision of 99.45%, Recall of 98.35%, F-score of 96.85%, Sensitivity of 99.4%, and Specificity of 97.98 % when compared to the existing Multi-input CNN that obtained accuracy of 93.8%, precision of 94.1%, Recall of 97.7%, F-score of 91.4%, Sensitivity of 88.9%, and specificity of 96.7%.

Keywords: Breast cancer, DenseNet 121 model, DMR-IR dataset, Hybrid statistical and texture feature extraction, Thermography.

1. Introduction

The breast disease study reported by the World Health Organization (WHO) confirms that breast cancer is the most impacted cancer occurred among women [1]. The study investigates the treatments and arrangements that support to enhancement of the cancer patient's survival rate [2]. Thermography is employed to diagnose breast cancer among patients. Thermography is employed for diagnosing breast cancer by using various instruments [3]. With respect to the thermographic techniques, deep neural networks have shown unequivocal potential for detecting the thermal patterns that are heterogeneous and relate to breast cancer cases [4]. The high dimensional thermal features extracted are called deep Thermomics. The studies conducted by various researchers show a comparison with the existing deep learning and neural networks to detect breast cancer [5]. The deep learning models are utilized for recommendations which showed a higher rate of accuracy compared to the neural networks [6]. The thermal imaging throughputs were extracted from the thermal images known as thermionics that are used extensively for delivering diagnostic solutions like radionics to detect early-stage breast cancers [7]. The thermionics techniques are companies with various

clinical variables which have shown improvement and also, the abundance of thermionics impedes by improving system's performances that lowered the overfitting and dimensionality problems [8, 9]. The thermal imaging and thermography images are obtained with the pain-free non-invasive method to detect a change in the breast that indicates breast cancer. The effective screening test is used for detecting breast cancer which shows the body part that detects the irregular temperature using the thermal infrared camera images. The thermography images transformed the infrared radiation signals into electrical signals [10]. The positive results obtained in the reviewed literature have limitations and challenges that are required to be overcome using Deep Learning (DL) and Machine Learning (ML) techniques for the classification and detection of breast cancer. The key challenges are reviewed with the inherent trends and directions for future study. The existing CNN model has diminished the higher level of neural network features. This problem is overcome by DenseNet 121, due to the longer path between the input layer and the output layer. The main advantage of using thermography apart from x-rays, CT scans, ultrasound, and MRI scans was because of their anatomical structure. The anatomical structure of the body has the unique ability to measure physiological changes. A huge data for training is present that has helped to improve the performance of the DL quality. The proposed research work is explained with the following contributions:

- To develop a DenseNet 121 that works well on cancer datasets for measuring the classification accuracy, specificity, and sensitivity.
- To develop a classification model for analyzing cancer prognosis by making use of the information including clinical data which is ignored by the present methods aimed at improving the prediction accuracies.

The organization of the paper is given as follows: Section 2 describes various existing research undergone for breast cancer detection. Section 3 explains the proposed method and the results and discussion of the proposed method are provided in Section 4. The conclusion of this research paper is given in Section 5.

2. Literature review

Raquel Sánchez-Cauce [11] developed a Multi-input Convolutional Neural Network (CNN) for the detection of breast cancer based on thermal images. The model was applied to the public database known as Database for Mastology Research (DMR) of breast thermal images for breast cancer detection. The model was exploited with the benefits of CNN to analyze the image. The personal and clinical data lacked homogeneity in DMR as it consists of a lot of information which were failed to analyze by the developed model.

Vartika Mishra and Santanu Kumar Rath [12] utilized feature reduction and classification algorithms for detecting breast cancer tumors based on thermos grams. Totally 56 subjects present at DMR for breast Thermo grams were considered for visual findings. The Gray Level Run Length Matrix (GLRLM) and Gray Level Co-occurrence Matrix (GLCM) texture features from images were extracted. The relevant observed features are selected to detect the abnormality among the unhealthy and healthy breast cancer images. The breast cancer thermography was restricted because of a lack of dataset availability with large thermos grams of a large number.

Subhrajit Dey [13] developed an edge detection aided deep transfer learning model to detect breast cancer from thermogram images. The DenseNet 121 model was pre-trained for extracting the features that build the classifiers. The two edge maps along with the original image consider feeding the input to the DenseNet 121 as a 3-channel image. The thermal breast image from the DMR dataset was used to evaluate the performance of the developed model. The developed model showed a problem in handling data imbalance as the model performances increased because of minority classes.

Asim Ali Khan and Ajat Shatru Arora [14] utilized Gabor features and ensemble classification for Early Detection of Breast Cancer. The double reading reduced the human errors that include interpretations of mammograms. The model detected automatically breast cancer that classified breast cancer into benign or abnormal cases. The low cost involved with thermography limited the resource communities which provided screening modalities in detecting breast cancer earlier.

Mathew Jose Mammoottil [15] developed Convolutional Neural Networks (CNN) for the detection of Breast Cancer from five viewed thermal images. The model was cost-effective and less invasive. The main objective of the model creates a machine learning model to detect breast cancer using the DMR dataset. The model utilized limited data and interacted with the data as it was not available.

Sourav Pramanik [16] developed an Arc-approximation and Triangular-space Search (BATS) to tackle the problem of breast regions. Initially, the breast region was segmented at the upper boundary (UB) of the breast using an arc approximation

algorithm. The Actual LBC of the breast region was traced with respect to the edge image by segmenting the IFR for the breast. However, the developed model failed to segment the region of the brain from the cases where the thermogram consisted of asymmetrical or insufficient fold regions of breasts

Mohammed Abdulla Salim Al Husaini [17] developed a Deep Convolutional Neural Network (DCNN) Inception MV4 which showed higher accuracy and improved operations. The developed model has set the thermal images that were sent to the smart phone and then to the cloud server. The model was evaluated from distinct distances and image acquisition procedures verified the image quality and the application of the method for early detection of breast cancer was required.

3. Proposed method

The block diagram of the proposed method is shown in Fig. 1 which includes the DMR-IR database which consisted of thermal images or infrared images. The thermal images are undergone the process of pre-processing using a Median Filter for the elimination of noise. The denoised images are undergone for the process of image segmentation using a multi-level Otsu thresholding approach. The segmented region undergoes the process of feature extraction using hybrid statistical and texture features. The hybrid statistic-texture-based features are fed for the Dense-Net model designed based on the CNN approach which classifies the thermal breast cancer image into the healthy or unhealthy image.

3.1 DMR data collection

The Database for Mastology Research (DMR) is an online platform that stores Mastology images to detect breast cancer. Mammography images are available that analyze MRI, ultrasound images, and thermal images by various research groups. The

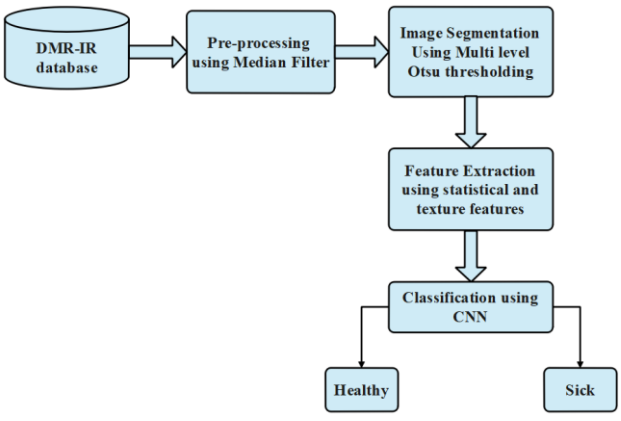

Figure. 1 Block diagram of the proposed research work

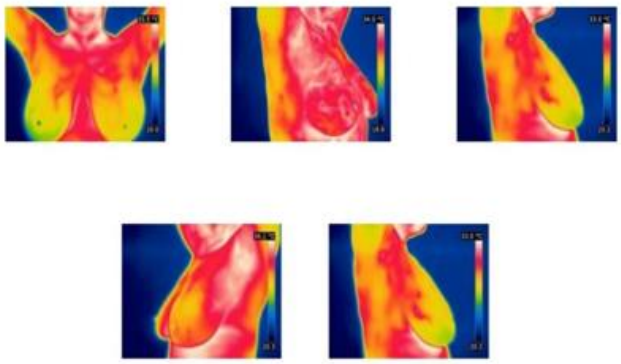

Figure. 2 Sample input images for the DRM-IR dataset

DMR-IR constitutes of IR images that are available with clinical data that is obtained from Hospital Universitário Antônio Pedro (HUAP) [18]. The acquisition protocols are having details as shown in the previous section. The dataset consists of a total 141 number of patients who are having the reports approved by the ethical committee. The IR images are present up to 3534 are summed with a total 27 number of patient images that were averagely obtained. The number of healthy images are 138 and sick images are 286. There is 5 number of distinct positions having the static protocol that consists of Front, Right Lateral 45°, Right Lateral 90°, Left Lateral 45° and Left Lateral 90°. The protocol generates around 20 sequential images that obtained dynamic protocol with front positions and 2 lateral images that consisted of (Right Lateral 90°, Left Lateral 90°). The present research uses the JPG image format for further processing. The sample input images for the DRM-IR databases is shown in Fig. 2.

3.2 Pre-processing using median filter

The dataset images collected are undergone the process of pre-processing using a median filter that converts thermal image pixels into grayscale pixels. It eliminates the unwanted parts of the breast image. The median filter is used for eliminating the noise and for conserving the edges. The model is extremely productive that eliminates the pepper and salt noises effectively. The median filter does not affect the image pixel as each of the values is not exchanged with the neighboring pixel value. The neighbors are called windows that glide the windows pixel by pixel over the image. The image median is firstly categorized by all the pixel values that consisted of a numerical sequence present as a window and once the pixel value is accounted the actual median pixel value is obtained. The median filtering algorithm instructs the window for arranging the pixel values by increasing or decreasing the sequences for median value selection. The median value is calculated by

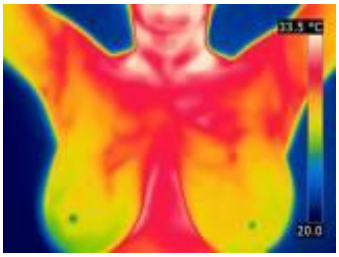

Figure. 3 Input image for Pre-processing

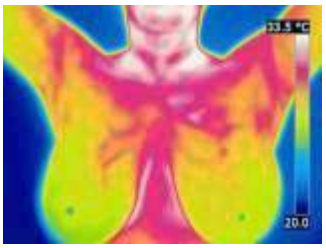

Figure. 4 Pre-processed images obtained by using median filter

averaging two middle values point windows. Fig. 3 shows the input image given from pre-processing stage. While Fig. 4 shows the pre-processed images that are obtained using a median filter.

3.3 Image segmentation

The pre-processed images are undergone for the process of segmentation by using Multi level Otsu thresholding approach. The segmentation is performed to binarize the image based on pixel intensities. The important regions are undergone for the process of segmentation using the thresholding approach that needs to be removed with the residue portion to detect it accurately. Thus, the function is performed with Multi-level Otsu thresholding which performed pixel separation for an input image that is having different classes for separating the gray levels based on the desired number. The main aim is to use multi-level Otsu thresholding and operator techniques to eliminate the unwanted regions. The unwanted regions are masked using the Morphology operation. The morphological operations are performed based on the sizes and shapes. The weights are calculated based on the class probabilities using Eq. (1)

$$q_1(t) = \sum_{i=1}^{t} P(i), \quad q_2(t) = \sum_{i=t+1}^{I} P(i), \quad q_n(t) = \sum_{i=I+t+1}^{n} P(i) \tag{1}$$

From the above Eq. (1), 1 to t is known as the threshold value, $q_{1\,..,n}$ is called the weighted class present among the pixel probabilities represented as P. The class means are given in Eq. (2)

$$\mu_1(t) = \sum_{i=1}^{t} \frac{iP(i)}{q_1(t)}, \mu_2(t) = \sum_{i=t=1}^{I} \frac{iP(i)}{q_2(t)}, \ldots\ldots, \mu_n(t) = \sum_{i=n}^{t} \frac{iP(i)}{q_n(t)} \tag{2}$$

μ_1 and μ_2 are called grey level values.

An input image has a structural element that is used to perform the morphological operations that obtain an output without losing the properties of an image. The morphological operations are performed on each input image pixel that is corresponded to the neighborhood pixels. The size and shape of an image are based on neighborhood pixels and morphological operations to construct the shapes of an input image specifically.

3.4 Hybrid feature extraction by using statistical and texture features

Once after segmenting the affected region, efficient hybrid features were utilized that integrated the statistical and texture features. The model was followed by extracting the features by the rotation of the images.

3.4.1. Statistical features

The statistical based feature selection model is used in evaluating the relationship among the target and input variables using the statistical features. The features are selected by the input variables that have the strongest relationship with the target variable.

3.4.1.1. Average energy

The Average Energy value is calculated by squaring the sum of the sampled values with the specified window time divided by the total sampled numbers present in the window. The Average Energy is expressed as shown in Eq. (3)

$$Average\ Energy = \sum_{i,j} \big(p(i,j)\big)^2 \tag{3}$$

3.4.1.2. Entropy

The value of entropy corresponds with the intensity levels that is having individual pixels for adapting. The entropy expression is provided as shown in Eq. (4)

$$Entropy = \sum_{i,j} p(i,j) \log_2 p(i,j) \tag{4}$$

3.4.1.3. Skewness

The term Skewness is defined as the symmetry measure which is precise lacked symmetry. The dataset or distribution is symmetric that looked

similar to that of the left and right of the center point. The univariate data $Y_1, Y_2 \dots, Y_N$ uses the skewness formula as shown in Eq. (5)

$$g_1 = \frac{\sum_{i=1}^{N} \frac{(Y_i - \bar{Y})^3}{N}}{s^3} \quad (5)$$

From the above Eq. (5), $\bar{Y}$ is called the mean, s is defined as the standard deviation, N is the data points. The computation of skewness is defined with the denominator as N rather than $N - 1$

3.4.1.4. Kurtosis

Kurtosis is defined as the measure of data that is tailed or lightly tailed relative to normal distributions. The univariate data is expressed as $Y_1, Y_2, \dots, Y_N$ which is defined as shown in Eq. (6)

$$kurtosis = \frac{\sum_{i=1}^{N} \frac{(Y_i - \bar{Y})^4}{N}}{s^4} \quad (6)$$

From the above Eq. (6), $\bar{Y}$ is called the mean, s is represented as the standard deviation, N is known as the data points. The skewness is a measure that is computed with the N with the denominator apart from $N - 1$. The term $p(i, j)$ is known as the image pixels row and column.

3.4.2. Texture features

The texture features are having visual patterns that consisted of spatially organized entities that had the characteristic of color, shape, brightness, and size. In images or portions of images where the pixel values are not varying much or are nearly similar, then the texture is said to be homogenous or smooth. On the other hand, varying pixels over a region depict a coarse texture. Textural features perform the local variation in intensity and are usually extracted from a single band. From different bands of texture features, the images are having generally distinct capabilities. Texture in an image can be perceived at different levels of resolution. Zooming out in an image makes an area smooth endowed compared with zooming in which locates all textural features. The image constituted of pixels are having various intensities with grey levels. The GLCM shows tabulation with how distinct values it forms a combination with green levels. The texture features utilize entries of the GLCM which provides a measure with intensity variation having a region of interest.

3.4.2.1. Contrast

Measures the gray levels q that vary in the image $I\ to$ that extent biased distribution. The mathematical expression for Contrast is shown in Eq. (7)

$$Contrast = \frac{\sigma}{(\alpha_4)^n} \quad (7)$$

From the above Eq. (8), $n = 0.25$ recommended, σ is known as the variance, α accounts degree of flatness

3.4.2.2. Homogeneity

The homogeneity feature is defined as the image textures which is scaled with local change in an image texture. The high-level homogeneity feature denotes the absence of intra-regional changes that distributes locally with the image textures.

3.4.2.3. Correlation

The correlation feature is defined as the process of moving the filter mask which is referred to as the kernel over an image I and the product sum of each location. Eq. (8) shows the expression for Correlation.

$$Correlation = F \cdot I(x) = \sum_{i=-N}^{N} F(i) I(x + i) \quad (8)$$

3.5 Classification using DenseNet 121 based CNN

The DenseNet-121 model is a CNN based model for the process of classification. The proposed model consisted of mainly 4 layers that are implanted as shown in Fig. 5. The DenseNet 121 is presented in Fig. 5 and the CNN model is started with an input image. The input image is applied to the filters to create the feature map. The l^{th} layer generates the feature maps such as $x_0, \dots, x_{l-1}$ from the upcoming layers and it is explained in Eq. (9).

$$X_l = H_l([X_0, X_1, \dots, X_{l-1}]) \quad (9)$$

Where $[X_0, X_1, \dots, X_{l-1}]$ is known as the feature maps that are concatenated and produced with layers ranging from 0, ..., $l - 1$. The activation function like ReLU is applied for increasing the non-linearity at the pooling layer when the feature maps were fed. The H_l the function generates the k level-based mapping features that are followed with l^{th} the layer which is evaluated using Eq. (10).

$$H_l = K_0 + K \times (L - 1) \quad (10)$$

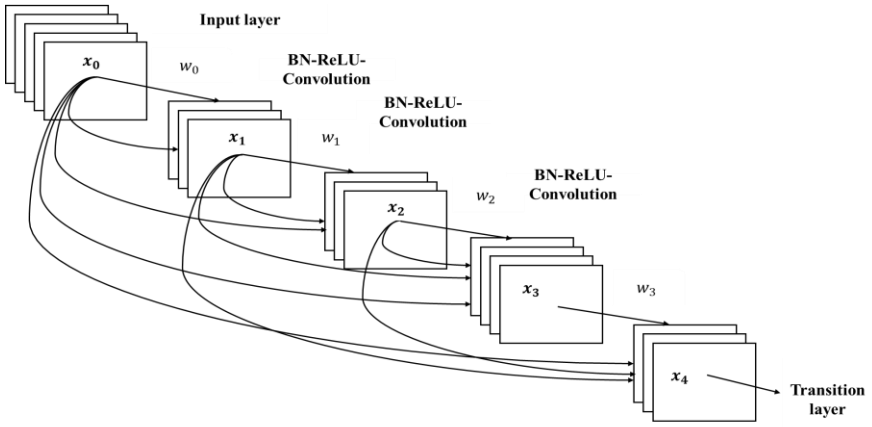

Figure. 5 Weighted dense net 121 model

From the above Eq. (10), K_0 is known as the overall number of channels that are present in the input layer. K is known as the hyperparameter having a better growth rate in the network. K feature maps are added at every layer having their own state. The computation of weights generated from the neuron is performed by the dot product and the computation of the input images is performed with respect to the volume.

The verification of activating the neurons to correct or not is based on ReLU layers. The random weights are assigned for the input layer which are represented as $w_0, w_1, w_2, \ldots, w_n$ that showed resultant features. From the above expression $n \in W$, where $W$is called the whole number. The generated output values obtained are undergone for training the weights at each of the transition layers. The ReLU is not changing to the dimension of the input image. Therefore, the pooling layer has lowered the noise level among the features that are extracted. The higher level of features was evaluated based on the outputs obtained in the FC layer. The deep CNN model uses DenseNet 121 for determining the position. The DenseNet 121 consists of 5 convolutional layers that learn around 13 weight layers. There are 4 FC layers and 2 Dense Net layers. The dropout regularization process is carried out by regularizing in the FC layer that is employed with an activation function. The obtained activation functions are fed to the convolutional layers which are expressed as shown in Eq. (11).

$$g_i^L = b_i^L + \sum_{j-1}^{m_1(L-1)} \psi_{i,j}^L \times h_j^{L-1} \tag{11}$$

From the above Eq. (11) g_i^L is known as the output layer represented as L, b_i^L represents the base value, $\psi_{i,j}^L$ is called as the filter connection with feature map, i^{th} level feature maps and j level features. h_j is the output layer having $L-1$ features. The model has reduced the unwanted features which solved the overfitting problem.

$$m_1^L = m_1^{L-1} \tag{12}$$

$$m_2^L = \frac{m_2^{L-1} - F(L)}{S^L} + 1 \tag{13}$$

$$m_3^L = \frac{m_3^{L-1} - F(L)}{S^L} + 1 \tag{14}$$

The Eqs. (12) to (14) have the ability to develop the feature map based on a transverse slice filter that removes the irrelevant features and overcomes the overfitting problems.

From the above Eqs. (15) and (16), S^L is known as the neural network parameters which changed the image movements that are expressed as m_1^L, m_2^L, m_3^L are feature maps that are obtained from the filter. The ReLU and FC are the other layers present, which are expressed as shown in Eqs. (15) and (16)

$$Re_i^l = \max(h, h_i^{l-1}) \tag{15}$$

$$FC_i^L = f\left(z_i^l\right) \text{ with } z_i^l = \sum_{j-1}^{m_1(l-1)} \sum_{s-1}^{m_2^{l-1}} \sum_{s-1}^{m_3^{l-1}} w_{i,j,r,s}^l \left(FC_i^{l-1}\right)_{r,s} \tag{16}$$

where, Re_i^l is called the ReLU layer, the output layer is represented as h, FC_i^L is called the FC layer is followed by the convolutional layers that evaluate the activation function. The DenseNet is used for feature reuse which is a central concept that results extremely with the compact versions. The intensity of the feature propagation has stimulated the turn down of the number of parameters that improved the accuracy of the model faster. The DenseNet has shown connectivity with each of the layers as easily as possible to connect each layer directly with the

other. The DenseNet-121 architecture has used the pre-trained weights and the foundation where the dense connections are essential with the feed-forward network. Thus, the Dense Net model showed an advantage over the other network models.

4. Results and discussions

The breast cancer detection using thermal images related paper implemented in MATLAB(2020a). The proposed method operates at windows 10, 16 GB RAM, i7 core processor, and 6GB 208- Ti NVDIA GTX where the edition is working with the GPU environments.

4.1 Performance measures

The results obtained by the proposed method are evaluated by the following parameter metrics.

4.1.1. Specificity

Specificity denotes is the true negative rate to the actual negative rate values to that of the corrected identified percentage. The expression for specificity is represented in Eq. (17)

$$Specificity(\%) = \frac{TN}{FP+TN} \times 100 \quad (17)$$

4.1.2. Sensitivity

Sensitivity is the measure of all the positive rates of the recall function to the detected probability detection function for the exact field which evaluated the positive values which is expressed as shown in Eq. (18).

$$Sensitivity(\%) = \frac{TP}{FN+TP} \times 100 \quad (18)$$

4.1.3. Accuracy

The systematic errors describe the statistical bias measures results with lower accuracy shows a huge difference as a result generates true values. Accuracy is expressed in Eq. (19)

$$Accuracy(\%) = \frac{TP+TN}{TP+TN+FP+FN} \times 100 \quad (19)$$

4.1.4. Precision

The term precision is defined as the truly predicted observations of the positive values for the total overall predicted observations. The precision is explained in Eq. (20)

$$Precision(\%) = \frac{TP}{TP+FP} \times 100 \quad (20)$$

4.1.5. Recall

Recall measure will indicate all the missed positive predictions which is defined using Eq. (21)

$$Recall(\%) = \frac{TP}{TP+FN} \times 100 \quad (21)$$

4.1.6. F-score

F-score is defined as the product of Precision and Recall that is defined as shown in the Eq. (22)

$$F - score\ (\%) = 2 \times \frac{Precision \times Recall}{Precision+Recall} \times 100 \quad (22)$$

4.2 Quantitative analysis

Table 1 shows the results obtained by the proposed hybrid statistical texture feature extraction with DenseNet 121 for the classification. The results were obtained by the statistical features such as Energy, Entropy, skewness, and kurtosis for ANN, DNN, CNN, and DenseNet 121 model in terms of accuracy, precision, recall, F-score, sensitivity, and specificity. ANN model data produced output with incomplete information. The ANN model showed a lack of performance as it was dependent on the importance of the information which was missing. The large training data was needed but failed to encode the position and orientation of the object by using the CNN model. The DNN model was hardware dependent and showed unexplained behavior in the network when the data were fed. Whereas, the DenseNet-121 has used the dense connections among the layers based on the dense blocks which are connected with all layers. Their matching the feature map sizes directly among each other showed improvement in the results. The DenseNet specifically improved and declined the accuracy which has caused the vanishing gradient with high-level neural networks. The model has shown simpler terms because of the longer path achieved among the input and the output layer. The information vanishes before the destination is reached. The results showed an accuracy of 60% for the Energy, Entropy of 72.54%, skewness of 87.31% and kurtosis of 87.88%, Contrast of 83.8%, Homogeneity of 84.9%, Correlation of 90% and hybrid features of 97.9%. Fig. 6 shows the graphical representation of the proposed method.

4.3 Comparative analysis

Table 2 shows the comparative analysis of the existing and the proposed models that are compared in terms of accuracy, precision, recall, f-score,

Table 1. Results obtained for the proposed hybrid features

Classifiers	Performances (%)	Hybrid features
ANN	Accuracy	94. 7
	Precision	94. 54
	Recall	94. 5
	F-score	94.8
	Sensitivity	94.8
	Specificity	94.9
DNN	Accuracy	95.9
	Precision	95.5
	Recall	95.65
	F-score	96.5
	Sensitivity	96.54
	Specificity	96.67
CNN	Accuracy	97.7
	Precision	97.45
	Recall	97.35
	F-score	97.85
	Sensitivity	97.4
	Specificity	97.98
Dense Net 121 (CNN)	Accuracy	98.97
	Precision	98.45
	Recall	95.35
	F-score	96.85
	Sensitivity	95.4
	Specificity	97.98

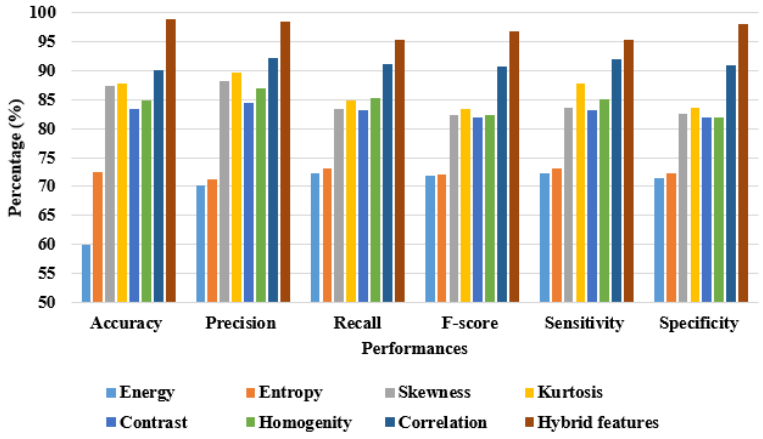

Figure. 6 Graphical representations of the proposed method

sensitivity, and specificity. The comparison is done for the proposed method based on the common database known as DMR-IR which consisted of infrared images for breast cancer detection. The proposed method obtained an accuracy of 98.97%, a precision of 99.45%, recall of 98.35%, f-score of 96.85 %, a sensitivity of 99.4%, and a specificity of 97.98%. As the proposed method used statistical features, the contralateral breast asymmetry is performed to detect an abnormality in breast cancer images. The texture feature extraction utilized in the present research work played an important role in performing the quantitative assessment. The breast thermogram for the minute detection of breast differences among them is performed based on the assessment. The DenseNet 121 is utilized for classifying the DMR-IR images which showed better results for huge data. The proposed DenseNet-121based CNN method is expressed as shown in Table 2. The most prevalent and seriously harmful type of sickness, particularly for women, is breast cancer. The primary goal of this study is to identify and classify breast cancer in women using ML which were knowledgeable about breast cancer prevention and willing to learn a computerized approach to problem-solving. Therefore, hybrid feature extraction with the Dense Net 121 model is proposed for solving the problem of breast cancer. The proposed method

Table 2. Comparative analysis

Methods	Accuracy (%)	Precision (%)	Recall (%)	F-score (%)	Sensitivity (%)	Specificity (%)
Multi-input convolutional Neural Network [11]	97	99	NA	NA	83	NA
RF-PCA [12]	95.45	94.28	NA	96.66	99.17	88.07
Gabor features and SVM classifier [14]	96.57	89.4	NA	91.89	NA	82.3
Multi-input CNN [15]	93.8	94.1	97.7	91.4	88.9	96.7
BATS [16]	95.75	NA	NA	95.34	91.88	99
DCNN[17]	98.72	NA	NA	NA	NA	NA
Proposed method	98.97	99.45	98.35	96.85	99.4	97.98

*NA – Not Available

provides high classification accuracy and efficient diagnostic abilities which are clearly illustrated in table 2. From the Table 2, it clearly shows that proposed method achieves the better accuracy (98.97%), precision (99.45%), Recall (98.35%), F-score (96.85%), Sensitivity (99.4%), and Specificity (97.98 %).

5. Conclusion

The present research work utilized a hybrid feature extraction model with the DenseNet 121 for classification. The main aim of using Hybrid feature extraction is to improve the learning rate of the DenseNet 121 that achieves better accuracy values. The proposed hybrid feature extraction technique constitutes of mainly two techniques as Statistical and texture feature extraction. The statistical features signified the breast asymmetry for detecting abnormal breast cancer detection. The texture-based features were utilized that played an important role in performing the quantitative assessment to the breast thermogram. The clinical data strengthen the prediction of breast cancer using the CNN technique which obtained 98.97 % of accuracy, a precision of 99.45%, Recall of 98.35%, F-score of 96.85%, Sensitivity of 99.4%, and Specificity of 97.98 % when compared to the existing Multi-input CNN that obtained accuracy of 93.8%, precision of 94.1%, Recall of 97.7%, F-score of 91.4%, Sensitivity of 88.9%, and specificity of 96.7%. In the future, thermography can be improved to detect breast cancer effectively for a standard database.

Conflicts of Interest

The authors declare no conflict of interest.

Author Contributions

The paper conceptualization, methodology, software, validation, have been done by 1st author formal analysis, investigation, resources, data curation have been done by 2nd author writing—original draft preparation, writing—review and editing, visualization, supervision and project administration, have been done by 3rd author.

Notation List

Notation	Description
t	Threshold value
$q_{1\ldots n}$	Weighted class
P	Pixel probability
μ_1 and μ_2	Grey level values
$Y_1, Y_2 \ldots, Y_N$	Univariate data
$\bar{Y}$	Mean
s	Standard deviation
N	Data points
$p(i,j)$	Pixel row and column
σ	Variance
α	Degree of flatness
$[X_0, X_1, \ldots, X_{l-1}]$	Feature maps
K_0	Overall number of channels
K	Hyper parameter
$w_0, w_1, w_2, \ldots, w_n$	Random weights
W	Whole number
g_i^L	Output layer
b_i^L	Base value
$\psi_{i,j}^L$	Filter connection with feature map
S^L	Neural network parameters
Re_i^l	ReLU layer
FC_i^L	FC layer
TP	True Positive
TN	True Negative
FP	False Positive
FN	False Negative

References

[1] Y. T. Acquaah, B. Gokaraju, R. C. Tesiero, and G. H. Monty, "Thermal Imagery Feature Extraction Techniques and the Effects on Machine Learning Models for Smart HVAC Efficiency in Building Energy", *Remote Sensing*, Vol. 13, No. 19, p. 3847, 2021.

[2] U. R. Gogoi, G. Majumdar, M. K. Bhowmik, A. K. Gzhosh, and D. Bhattacharjee, "Breast abnormality detection through statistical feature analysis using infrared thermograms", In: *Proc. of 2015 International Symposium on Advanced Computing and Communication (ISACC)*, pp. 258-265, 2015.

[3] A. Ibrahim, S. Mohammed, H. A. Ali, and S. E. Hussein, "Breast cancer segmentation from thermal images based on chaotic salp swarm algorithm", *IEEE Access*, Vol. 8, pp. 122121-122134, 2020.

[4] İ. SekmenoĞlu, M. M. AkgÜl, and S. İÇer, "Classification of Thermal Breast Images Using Support Vector Machines", In: *Proc. of 2021 Medical Technologies Congress (TIPTEKNO)*, pp. 1-4, 2021.

[5] V. Mishra and S. K. Rath, "Detection of breast cancer tumours based on feature reduction and classification of thermograms", *Quantitative InfraRed Thermography Journal*, Vol. 18, No. 5, pp. 300-313, 2021.

[6] S. Ervural and M. Ceylan, "Thermogram classification using deep siamese network for neonatal disease detection with limited data", *Quantitative InfraRed Thermography Journal*, pp. 1-19, 2021.

[7] M. Macedo, M. Santana, W. P. D. Santos, R. Menezes, and C. B. Filho, "Breast cancer diagnosis using thermal image analysis: A data-driven approach based on swarm intelligence and supervised learning for optimized feature selection", *Applied Soft Computing*, Vol. 109, p. 107533, 2021.

[8] S. Niu, X. Zhang, G. R. Williams, J. Wu, F. Gao, Z. Fu, X. Chen, S. Lu, and L. M. Zhu, "Hollow mesoporous silica nanoparticles gated by chitosan-copper sulfide composites as theranostic agents for the treatment of breast cancer", *Acta Biomaterialia*, Vol. 126, pp. 408-420, 2021.

[9] R. Resmini, L. F. D. Silva, P. R. Medeiros, A. S. Araujo, D. C. M. Saade, and A. Conci, "A hybrid methodology for breast screening and cancer diagnosis using thermography", *Computers in Biology and Medicine*, Vol. 135, p. 104553, 2021.

[10] N. K. Chebbah, M. Ouslim, and S. Benabid, "New computer aided diagnostic system using deep neural network and SVM to detect breast cancer in thermography", *Quantitative InfraRed Thermography Journal*, pp. 1-16, 2022.

[11] R. S. Cauce, J. P. Martín, and M. Luque, "Multi-input convolutional neural network for breast cancer detection using thermal images and clinical data", *Computer Methods and Programs in Biomedicine*, Vol. 204, p. 106045, 2021.

[12] V. Mishra and S. K. Rath, "Detection of breast cancer tumours based on feature reduction and classification of thermograms", *Quantitative InfraRed Thermography Journal*, Vol. 18, No. 5, pp. 300-313, 2021.

[13] S. Dey, R. Roychoudhury, S. Malakar, and S. Sarkar, "Screening of breast cancer from thermogram images by edge detection aided deep transfer learning model", *Multimedia Tools and Applications*, pp. 1-19, 2022.

[14] A. A. Khan and A. S. Arora, "Thermography as an Economical Alternative Modality to Mammography for Early Detection of Breast Cancer", *Journal of Healthcare Engineering*, pp. 2021, 2021.

[15] M. J. Mammoottil, L. J. Kulangara, A. S. Cherian, P. Mohandas, K. Hasikin, and M. Mahmud, "Detection of Breast Cancer from Five-View Thermal Images Using Convolutional Neural Networks", *Journal of Healthcare Engineering*, 2022.

[16] S. Pramanik, S. Ghosh, D. Bhattacharjee, and M. Nasipuri, "Segmentation of breast-region in breast thermogram using arc-approximation and triangular-space search", *IEEE Transactions on Instrumentation and Measurement*, Vol. 69, No. 7, pp. 4785-4795, 2019.

[17] M. A. S. A. Husaini, M. H. Habaebi, T. S. Gunawan, and M. R. Islam, "Self-Detection of Early Breast Cancer Application with Infrared Camera and Deep Learning", *Electronics*, Vol. 10, No. 20, p. 2538, 2021.

[18] A. Conci, R. C. F. Lima, R. C. Serrano, L. S. Motta, and R. H. C. Mello, "Using fractal geometry to extract features of thermal images for early breast diseases", In: *Proc. of 14th International Conference on Geometry and Graphics*, pp. 208-217, 2010.

[19] G. L. Menezes, R. M. Mann, C. Meeuwis, B. Bisschops, J. Veltman, P. T. Lavin, M. J. V. D. Vijver, and R. M. Pijnappel, "Optoacoustic imaging of the breast: correlation with histopathology and histopathologic biomarkers", *European Radiology*, Vol. 29, No. 12, pp. 6728-6740, 2019.

[20] A. Paul, A. Gangopadhyay, A. R. Chintha, D. P. Mukherjee, P. Das, and S. Kundu, "Calculation of phase fraction in steel microstructure images using random forest classifier", *IET Image Processing*, Vol. 12, No. 8, pp. 1370-1377, 2018.
[21] Y. Li, X. Zhu, and J. Liu, "An improved moth-flame optimization algorithm for engineering problems", *Symmetry*, Vol. 12, No. 8, p. 1234, 2020.
[22] O. Fallahzadeh, Z. D. Bidgoli, and M. Assarian, "Raman spectral feature selection using ant colony optimization for breast cancer diagnosis", *Lasers in Medical Science*, Vol. 33, No. 8, pp. 1799-1806, 2018.
[23] J. Xu, X. Luo, G. Wang, H. Gilmore, and A. Madabhushi, "A deep convolutional neural network for segmenting and classifying epithelial and stromal regions in histopathological images", *Neurocomputing*, Vol. 191, pp. 214-223, 2016.
[24] E. Rezk, Z. Awan, F. Islam, A. Jaoua, S. A. Maadeed, N. Zhang, G. Das, and N. Rajpoot, "Conceptual data sampling for breast cancer histology image classification", *Computers in Biology and Medicine*, Vol. 89, pp. 59-67, 2017.
[25] Y. Feng, L. Zhang, and Z. Yi, "Breast cancer cell nuclei classification in histopathology images using deep neural networks", *International Journal of Computer Assisted Radiology and Surgery*, Vol. 13, No. 2, pp. 179-191, 2018.